Nucl Eng Technol 47 (2015) 398–406

Available online at www.sciencedirect.com

ScienceDirect

journal homepage: http://www.journals.elsevier.com/nuclear-engineering-and-technology/

Invited Article

EFFECTS OF AL_2O_3 NANOPARTICLES DEPOSITION ON CRITICAL HEAT FLUX OF R-123 IN FLOW BOILING HEAT TRANSFER

*SEOK BIN SEO and IN CHEOL BANG**

School of Mechanical and Nuclear Engineering, Ulsan National Institute of Science and Technology (UNIST), Number 50, UNIST-gil, Ulju-gun, Ulsan 689-798, Republic of Korea

ARTICLE INFO

Article history:
Received 27 February 2015
Received in revised form
7 April 2015
Accepted 8 April 2015
Available online 22 April 2015

Keywords:
Boiling heat transfer
Chalk River unidentified deposit
Critical heat flux
Nanofluid
Porous structure

ABSTRACT

In this study, R-123 flow boiling experiments were carried out to investigate the effects of nanoparticle deposition on heater surfaces on flow critical heat flux (CHF) and boiling heat transfer. It is known that CHF enhancement by nanoparticles results from porous structures that are very similar to layers of Chalk River unidentified deposit formed on nuclear fuel rod surfaces during the reactor operation period. Although previous studies have investigated the surface effects through surface modifications, most studies are limited to pool boiling conditions, and therefore, the effects of porous surfaces on flow boiling heat transfer are still unclear. In addition, there have been only few reports on suppression of wetting for decoupled approaches of reasoning. In this study, bare and Al_2O_3 nanoparticle-coated surfaces were prepared for the study experiments. The CHF of each surface was measured with different mass fluxes of 1,600 kg/m^{2}s, 1,800 kg/m^{2}s, 2,100 kg/m^{2}s, 2,400 kg/m^{2}s, and 2,600 kg/m^{2}s. The nanoparticle-coated tube showed CHF enhancement up to 17% at a mass flux of 2,400 kg/m^{2}s compared with the bare tube. The factors for CHF enhancement are related to the enhanced rewetting process derived from capillary action through porous structures built-up by nanoparticles while suppressing relative wettability effects between two sample surfaces as a highly wettable R-123 refrigerant was used as a working fluid.

Copyright © 2015, Published by Elsevier Korea LLC on behalf of Korean Nuclear Society.

1. Introduction

Boiling is an effective heat transfer mode and has high heat transfer capacity through phase transformation. Many thermal applications, including nuclear power plants, utilize the phenomenon of boiling in their heat-removal processes. However, the efficient boiling heat transfer is limited by a sudden and drastic reduction of the heat transfer coefficient

* *Corresponding author.*
E-mail address: icbang@unist.ac.kr (I.C. Bang).

This is an Open Access article distributed under the terms of the Creative Commons Attribution Non-Commercial License (http://creativecommons.org/licenses/by-nc/3.0) which permits unrestricted non-commercial use, distribution, and reproduction in any medium, provided the original work is properly cited.

http://dx.doi.org/10.1016/j.net.2015.04.003

1738-5733/Copyright © 2015, Published by Elsevier Korea LLC on behalf of Korean Nuclear Society.

due to the vapor blocking phenomena around a heated surface, called critical heat flux (CHF). Beyond the CHF, the heated surface will be exposed to only vapor environment, and it could result in excessive heating and physical failure of the heated surface, called burnout. Especially in nuclear reactors, the CHF directly affects the integrity of the core. Thus, understanding CHF mechanisms and enhancing CHF provide an additional safety margin for the reactor, and can also enable power uprates in commercial nuclear power plants [1]. For a pressurized water reactor (PWR), the main CHF mechanism is departure from nucleate boiling (DNB) whose characteristics are high mass flow rate and low quality. Thus, it is necessary to understand the physical model of DNB to ensure the safety of PWRs. The widely accepted models were proposed by Weisman and Pei [2] and Lee and Mudawwar [3]. One is the near-wall bubble crowding model based on enthalpy transportation through the interface between the boundary layer and the bulk core. The other is the liquid sublayer dryout model, which introduces a liquid sublayer located between the vapor blanket and the heated surface. In the liquid sublayer dryout model, the dry patch is generated from the vapor blanket contacting the heated wall as a result of Helmholtz instability. Near CHF, the dry patch spreads over the wall, when the rate of sublayer mass loss by evaporation exceeds that of the liquid entering the sublayer from the core region.

Many enhancement techniques have been introduced to increase CHF in a nuclear reactor. Using nanofluid to increase CHF is a relatively new method, which enhances the boiling heat transfer and CHF [4]. Early studies using different nanofluids have reported significant enhancement of CHF in pool boiling up to 200% [5–9]. CHF enhancement by nanofluids in flow boiling, which is the condition of interest for nuclear applications, has also been investigated [10–13]. Relatively few studies about flow boiling using nanofluids have been reported, compared to those about pool boiling, and the maximum enhancement was lower than that of pool boiling condition. The previous studies referred to a nanoparticles-deposited layer on the heating surface as the main factor of CHF enhancement. However, the mechanism of CHF enhancement has yet to be clarified and is still under debate.

Although using nanofluid is as an effective technique to enhance CHF inflow boiling, its feasibility for nuclear applications seems to be low due to its stability and deposition/cleaning issues. Instead of the nanofluid, nanoparticle-coated heating surfaces have been considered as an alternative method for CHF enhancement. In addition, the nanoparticle-coated heating surface can be a more meaningful technique, because it has similar characteristics with Chalk River unidentified deposits (CRUDs) on the cladding surface in an actual nuclear reactor. CRUDs are corrosion products deposited on the cladding surface during the normal operation of a nuclear power plant [14,15]. These products form a microstructured layer providing beneficial effects on the boiling heat transfer coefficient and CHF. In general, CRUD is a porous structure made of hydrophilic particles, which is similar to nanoparticle-coated structures [16]. Thus, investigation of nanoparticle-coated structures can be extended to CRUD structures, leading to clear prediction of CHF enhancement in actual nuclear reactors.

Few studies have focused on the CHF enhancement by nanoparticle-coated surfaces in the flow boiling condition. Sarwar et al. [17] conducted a flow boiling experiment on a coated surface. The authors coated Al_2O_3 and TiO_2 nanoparticles inside a circular tube using the coating paint technique. The nanoparticle-coated surface showed a porous structure, which is similar to depositions formed on the heated surfaces in previous nanofluid-boiled experiments. In addition, the measured CHFs were enhanced up to 25% compared with those on the smooth tube. Truong et al. [18] also precoated Al_2O_3 nanoparticles inside a tube to investigate CHF enhancement. The test parameters included the coating concentration of the nanofluid, coating heat flux, and coating time. The maximum CHF enhancement occurred in the condition of the highest coating concentration, coating heat flux, and coating time with a value of 35%. Kim et al. [19] measured the flow boiling CHFs in two conditions: Al_2O_3 nanofluid boiled through a plain tube and pure water boiled through an Al_2O_3 nanoparticle-coated tube. In both cases, CHFs were enhanced compared with CHF on a water-boiled plain tube, and there was no big difference in CHF results between the two conditions. These results confirmed that the deposition of nanoparticles on the heating surface leads to CHF enhancement.

While early studies mainly focused on wettability of the heating surface for CHF enhancement, both the surface morphology and wettability have been considered only recently [11,13]. Because the surface characteristics are closely coupled to each other, it is crucial that those parameters are decoupled as much as possible. In that sense, we used refrigerant R-123 as a working fluid for the CHF measurement in this study. Although the refrigerant R-123 has been used mainly for flow boiling in microtubes to investigate parametric effects and flow regime [20–22], this study used a millimeter-sized cylindrical tube to investigate the CHF enhancement mechanism. The highly wettable characteristic of the refrigerant was expected to suppress the wettability effect of the nanoparticle-coated heating surface on the CHF, and therefore, surface morphology including porosity and roughness was assumed to be responsible for CHF enhancement [23]. Finally, in this study, CHF enhancement on an Al_2O_3 nanoparticle-coated surface was measured with different mass flux conditions, and its mechanisms were analyzed based on previous CHF models in terms of the liquid sublayer.

2. Experimental procedure

A schematic diagram of the experimental facility is shown in Fig. 1. The flow loop consists of a test section, a pump, a flowmeter, a preheater, a condenser, and a fluid reservoir. A controlled volume pump is used for a low mass flow rate ranging from 0.037 to 0.061 kg/s. The corresponding mass flux is in the range from 1,600 kg/m^{2}s to 2,800 kg/m^{2}s. The gear flowmeter measures mass flow rate using rotating gears in the liquid flow. After passing the mass flowmeter, the coolant flows to the preheater to maintain constant inlet temperature. The condenser has a capacity of 11 kW, which is enough to remove applied heat from the test section.

Stainless steel 316L tubes of 5.45-mm inner diameter were used as the test heaters. The heating length is 280 mm. The

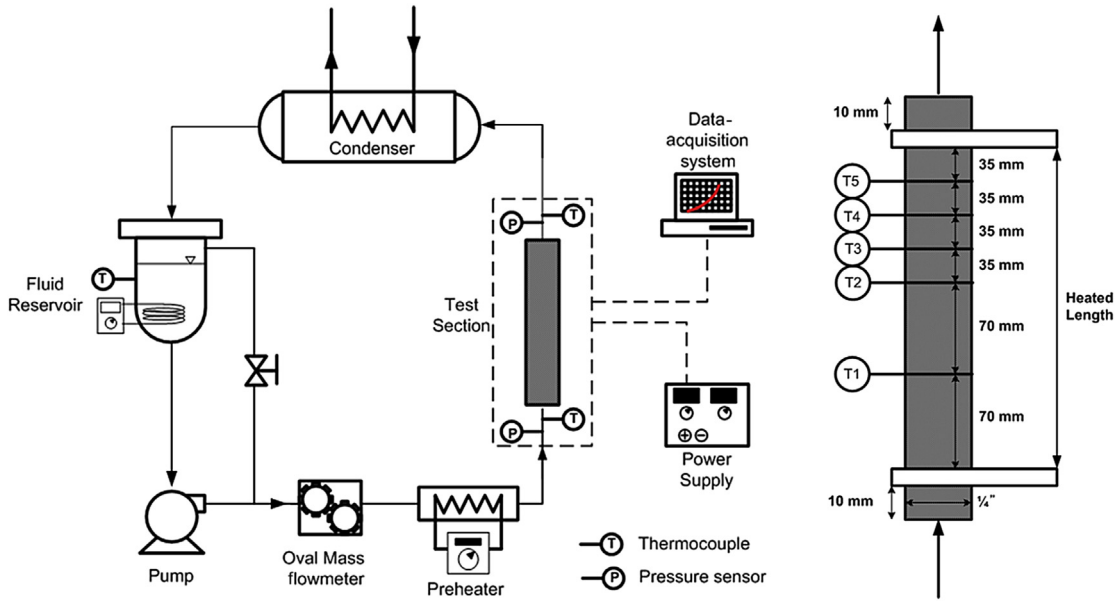

Fig. 1 – Schematic diagram of the testing apparatus.

working fluid is R-123, which has a low boiling temperature of 26°C at atmospheric pressure. The detailed test matrix of the experiment is listed in Table 1. The fluid temperatures at the inlet and outlet of the test section were measured by K-type thermocouples, which were connected to a data-acquisition system. Another five K-type thermocouples were installed to measure the outer wall temperatures of the tube. CHF occurs near the exit of the test section due to axially uniform heat flux. When a wall temperature excursion takes place, the heat flux value at that point becomes the CHF. The determination of CHF based on the wall temperature excursion is shown in Fig. 2.

Table 1 – Test matrix of the experiment.

Test section characteristics	
Geometry	Stainless steel 316L cylindrical tube
Outer diameter	6.35 mm
Inner diameter	5.45 mm
Heated length	280 mm
Surface conditions	
Bare	–
Coated	900-s quenching with 0.01 vol% Al_2O_3 nanofluid
Vertically upward flow	
Pressure	1 bar
Mass flux	1,600 kg/m^{2}s, 1,800 kg/m^{2}s, 2,100 kg/m^{2}s, 2,400 kg/m^{2}s, and 2,600 kg/m^{2}s
Inlet subcooling	5°C
Working fluid	R-123
Density	1,460 kg/m^3 (liquid) 6.41 kg/m^3 (vapor)
Latent heat	170.2 kJ/kg
Heat capacity	1.026 kJ/kgK

3. Data reduction and uncertainties

The voltage, current, inlet and outlet fluid temperatures, wall temperature, and inlet and outlet pressures were measured. The electrical input power applied to the test section was determined with measured voltage and current from the power supply:

$$Q_{net} = V \times I \tag{1}$$

The inner wall temperature of the test section is calculated as follows:

$$T_{wall} = T_{wall,out} - \dot{Q}_{net}\frac{\ln(D_0 - D_i)}{2\pi L_{eff,h} k_c} \tag{2}$$

where the actual CHF corresponding to the inner surface area of the test section is expressed as follows:

$$q''_{eff} = \frac{P}{\pi D_i L_{eff,h}} \tag{3}$$

Finally, the exit quality can be calculated with the mass flow rate and net power derived from the phase change as heat balance:

$$X_e = \frac{1}{h_{fg}}\left[\frac{\dot{Q}_{net}}{\dot{m}_f} - c_{p,f}(T_{sat} - T_{in})\right] \tag{4}$$

The uncertainties of temperature and flow rate are less than ±0.5 °C and ±5%, respectively. In addition, the uncertainties in the electrical voltage, current, inner diameter, and length of test section are estimated to be ±0.3%, ±0.08%, ±0.1%, and ±1%, respectively. Finally, the uncertainty in the CHF is evaluated as follows:

$$\frac{U_{q''}}{q''} = \sqrt{\left(\frac{U_V}{V}\right)^2 + \left(\frac{U_I}{I}\right)^2 + \left(\frac{U_{D_i}}{D_i}\right)^2 + \left(\frac{U_L}{L}\right)^2} \tag{5}$$

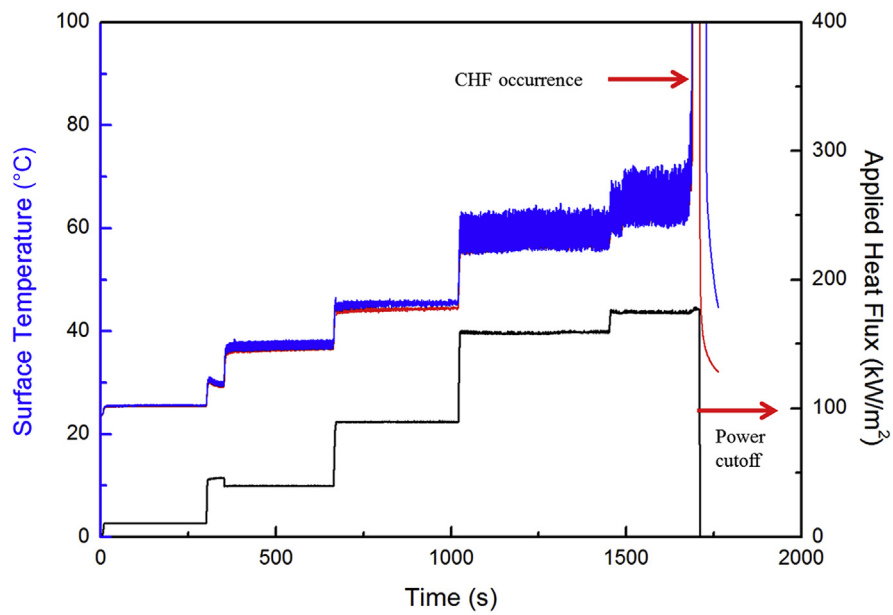

Fig. 2 – Wall temperature and heat flux history in a typical critical heat flux (CHF) run.

Therefore, the measurement uncertainty of the calculated CHF is less than ±1.05%.

4. Characterization of nanoparticle-coated surface

In general, the major parameters to characterize a surface treatment are wettability, roughness, and porosity, as well as permeability and capillarity. The capillary action or capillarity relationship depends on the interaction of wettability, pore structure, initial saturation, and saturation history, which is liquid distribution inside the pore structure [24]. No simple relationship exists that relates the capillary pressure determined at two different wettabilities. The surface effects on boiling heat transfer and CHF mechanisms are summarized in Table 2.

In this study, nanoparticles were coated on the inner surface of a tube at a quenching facility at Ulsan National Institute of Science and Technology (UNIST). Previous studies with the quenching method at UNIST have shown the stability and maintenance of the nanoparticle-coated structure inside the tube [25]. Nanofluids (0.01 vol%) were injected at a flow rate of 3 cm/s into the preheated test section (600–650°C) to deposit the nanoparticles on the inner surface of the test section. The circulation of nanofluids lasted for 900 seconds. The boiling process induces the coating of nanoparticle on the test section. The adhesion force is significant to maintain the deposition of nanoparticles on the surface against the flow of water.

Fig. 3 shows scanning electron microscopy images of the bare and nanoparticle-coated test sections. Compared with the bare surface in Fig. 3A, Al_2O_3 nanoparticles-coated surfaces show a number of pores on the surface as shown in Fig. 3B. In addition, from Fig. 3B and C, it is certain that most of the deposited nanoparticles remained for all the experiments. From the perspective view of the nanoparticle-coated surface shown in Fig. 4, the nanoparticle-coated test section shows a very rough and porous structure on the bare surface.

Table 2 – Summary of the major surface parameters on boiling heat transfer and critical heat flux mechanism.

Surface parameters	Characteristics	Quantification (measurement)
Wettability	Determines the wetting zone on the surface, rewetting	Contact angle (°)
Roughness	Affects the number of active nucleation sites on the surface Increases active boiling center Amplifies for wettability	Surface's vertical deviation (m)
Porosity	Increases the nucleation site density Enhances transport of liquid between nucleation sites Thick porous layer can provide additional thermal resistance	Void fraction
Permeability	The property of pore structure that is an indication of the ability of gases or fluids to flow through the structure	Forced liquid flow (m^2)
Capillarity	Affects liquid supply to the dry patches on the surface induced by the capillary action	Capillary height or length (m)

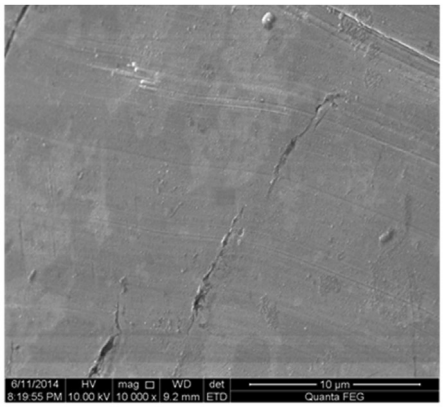

(A)

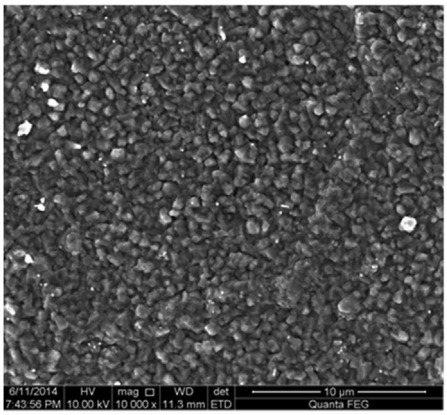

(B)

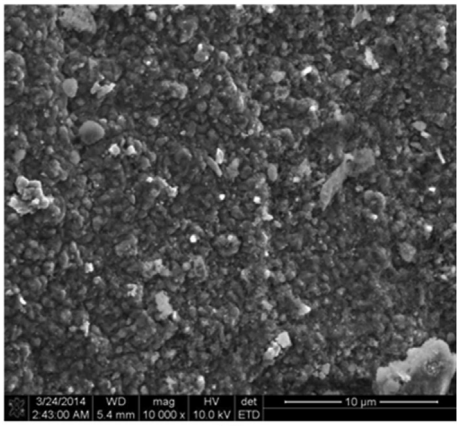

(C)

Fig. 3 – Scanning electron microscopy images of bare and Al_2O_3 nanoparticle-coated surface: (A) bare surface; (B) Al_2O_3 nanoparticle-coated surface before the experiment; (C) Al_2O_3 nanoparticle-coated surface after the experiment.

The R-123 droplets on the bare and nanoparticle-coated surfaces were used to measure the static contact angle. The static contact angle for the bare surface was 20.5°, whereas those for the nanoparticle-coated surfaces were 22.3°. This indicates that R-123 shows very high wetting performance on both bare and nanoparticle-coated tubes. The measured static contact angles are shown in Fig. 5.

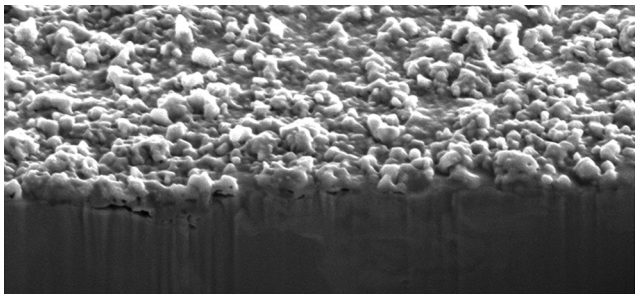

Fig. 4 – Cross-sectional view of Al_2O_3 nanoparticle-coated surface using the FIB technique.

5. Results and discussion

In this paper, the effects of deposition of nanoparticles on flow boiling CHF using R-123 were investigated. The mass flux conditions (G) are 1,600 kg/m^{2}s, 1,800 kg/m^{2}s, 2,100 kg/m^{2}s, 2,400 kg/m^{2}s, and 2,600 kg/m^{2}s at the inlet subcooled temperature of 5°C. Based on the liquid sublayer model, CHF enhancement by nanoparticle-coated surface is analyzed.

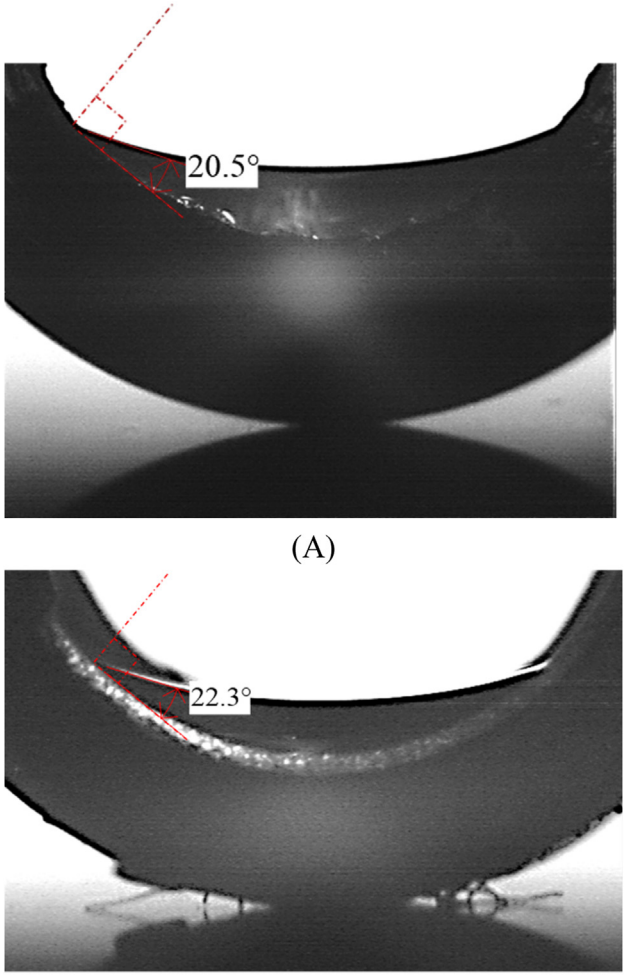

Fig. 5 – Static contact angle of R-123: (A) bare surface; (B) Al_2O_3 nanoparticle-coated surface.

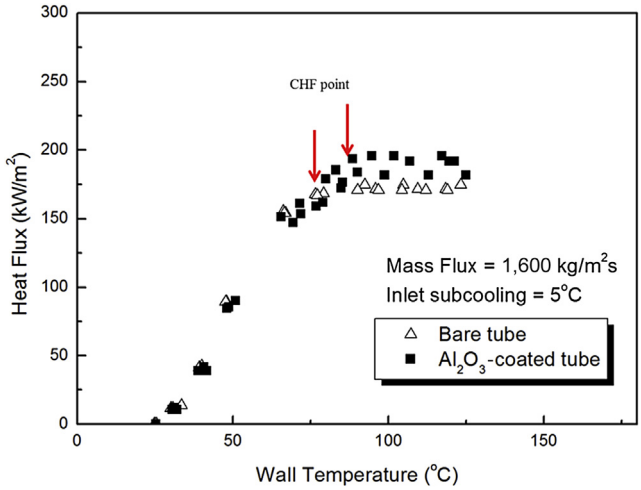

Fig. 6 – Boiling curves for bare tube and Al_2O_3-coated tube at G = 1,600 kg/m²s. CHF, critical heat flux.

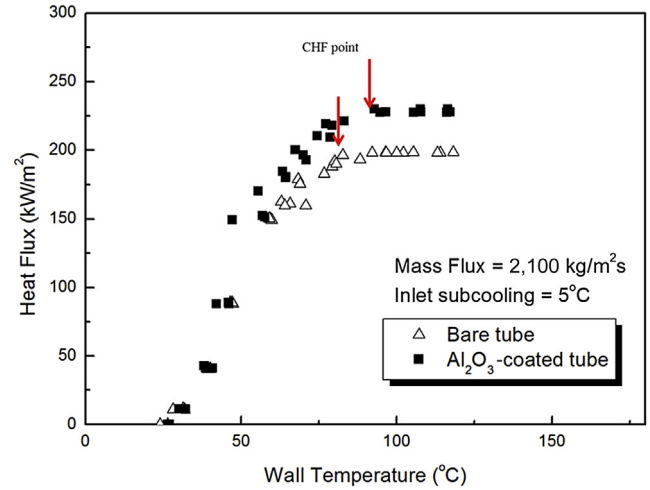

Fig. 8 – Boiling curves for bare tube and Al_2O_3-coated tube at G = 2,100 kg/m²s. CHF, critical heat flux.

The flow boiling experiments using R-123 were conducted on the bare and nanoparticle-coated heaters at the given mass fluxes. Heat flux versus wall temperature was plotted at each mass flux. The boiling curves obtained at different mass fluxes are shown in Figs. 6–10. As the mass flux increased, the heat transfer coefficient, which refers to the slope of the boiling curve, also increased. However, near the CHF point, the heat transfer coefficient decreased and then became almost zero slope after the CHF point where the wall temperature kept increasing with constant heat flux. At the higher mass flux conditions over 2,100 kg/m², the heat transfer coefficients increased for the Al_2O_3 nanoparticle-coated tube compared with those for the bare tube. The increase in the heat transfer coefficients was up to 50% for the Al_2O_3 nanoparticle-coated tube compared with those for the bare tube at G = 2,100 kg/m². Because the heat transfer coefficient is highly dependent on surface wettability and coating layer thickness, and slightly

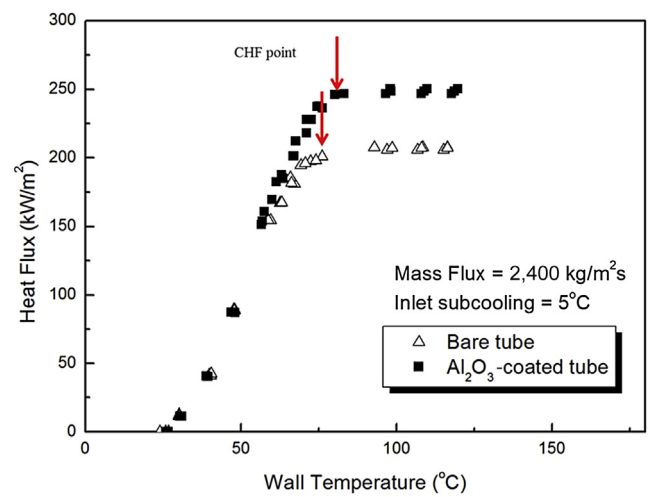

Fig. 9 – Boiling curves for bare tube and Al_2O_3-coated tube at G = 2,400 kg/m²s. CHF, critical heat flux.

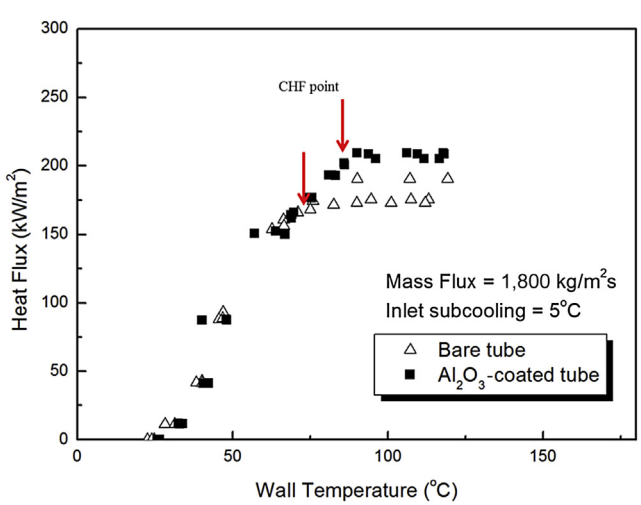

Fig. 7 – Boiling curves for bare tube and Al_2O_3-coated tube at G = 1,800 kg/m²s. CHF, critical heat flux.

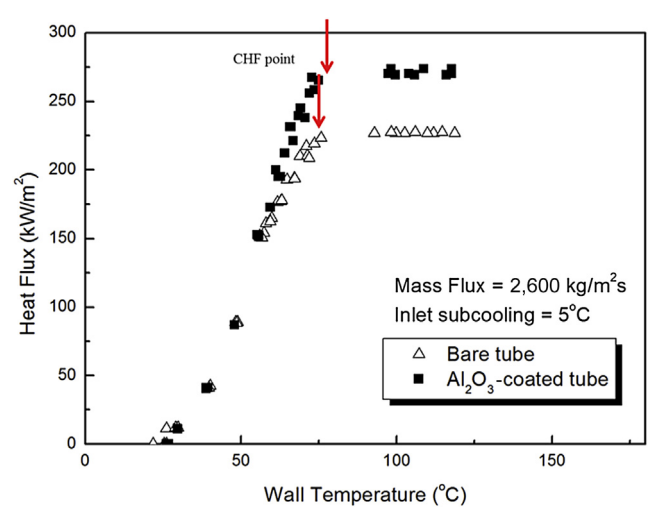

Fig. 10 – Boiling curves for bare tube and Al_2O_3-coated tube at G = 2,600 kg/m²s. CHF, critical heat flux.

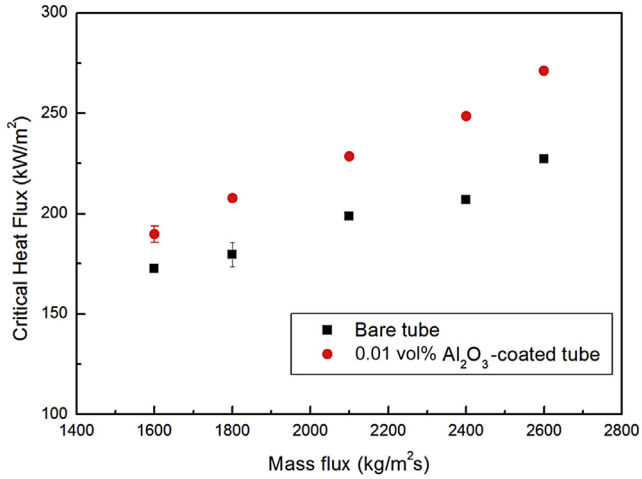

Fig. 11 – Critical heat flux of R-123 on the bare and Al_2O_3 nanoparticle-coated test sections with mass flux.

dependent on surface morphology [26], the increase of the heat transfer coefficient for the coated tube may be attributed to the porous structure formed by Al_2O_3 nanoparticles.

The CHF data obtained on bare and nanoparticle-coated surfaces according to mass fluxes are shown in Fig. 11. As the mass flux increases, CHF increased due to the larger heat capacity and better liquid supply of fluid. The parametric trend is also shown for the nanoparticle-coated surface. Interestingly, for all mass flux conditions, the CHFs were enhanced on the Al_2O_3 nanoparticle-coated surfaces compared with the bare surface, even when the coating layer thickness is in the nano-scale level, approximately 300 nm. The nanoparticle-coated surface shows CHF enhancement up to 17% compared with the bare surface for each corresponding mass flux condition. Considering the high wettability performance of R-123, those CHF enhancements are attributed to structural changes, especially porous structures formed by deposited nanoparticles. Fig. 12 shows the flow boiling CHF enhancement ratios, which are defined as the ratio of CHF on the Al_2O_3 nanoparticle-coated surface to CHF on the bare surface, with an increasing mass flux from 1,600 kg/m^{2}s to 2,600 kg/m^{2}s.

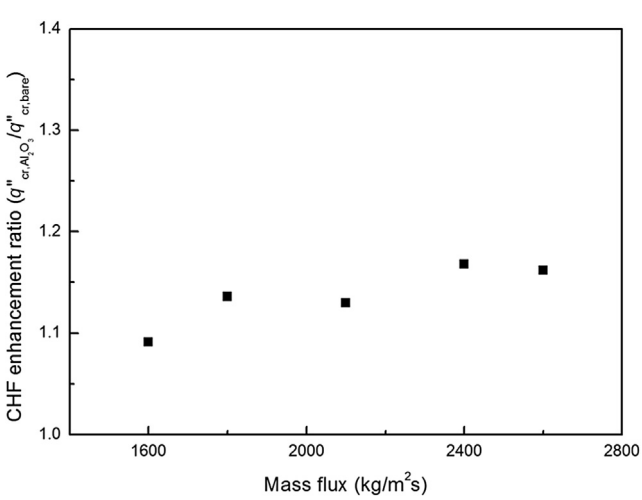

Fig. 12 – Critical heat flux (CHF) enhancement ratio of R-123 with mass flux.

Based on the sublayer dryout model [3], interruption of liquid supply to the sublayer enlarges the dry patches leading to CHF. Then, maintenance of liquid supply to the sublayer after detaching the vapor bubble, called the rewetting process, can delay CHF. Assuming the liquid supply is pumped by capillary force and gravitational force, the pressure drop by the liquid flow through the pores can be modeled using the Darcy–Ergun momentum relation [27,28]:

$$-\nabla p_l + \rho_l \widehat{g} - \frac{\mu_l}{K}\langle \widehat{u}_l \rangle - \frac{C_E}{K^{1/2}}\rho_l |\langle \widehat{u}_l \rangle| \langle \widehat{u}_l \rangle = 0 \tag{6}$$

where p_l is the liquid pressure, ρ_l is the liquid density, μ_l is the dynamic viscosity of liquid, $\langle u_l \rangle$ is the volume-averaged liquid velocity vector through the liquid-saturated region within the porous-layer coating, K is the media permeability, and C_E is the Ergun coefficient. K and C_E are defined by the Carmen–Kozeny model:

$$K = \frac{\varepsilon^3 d^2}{180(1-\varepsilon)^2} \tag{7}$$

$$C_E = \left(\frac{0.018}{\varepsilon^3}\right)^{1/2} \tag{8}$$

where ε is porosity, and d is the diameter of porous particles.

To reduce the Darcy–Ergun momentum relation to a function of porous structure, the Leverett J-function was introduced. The Leverett J-function expresses the capillary pressure through a porous stack using the liquid saturation (s), porosity, permeability, and wettability [27].

$$p_g - p_l = p_c = J(s)\frac{\sigma \cos\theta_c Z(\theta_c)}{(K/\varepsilon)^{1/2}} = C_J \frac{\sigma}{(K/\varepsilon)^{1/2}} \tag{9}$$

where p_g is the vapor pressure, p_c is the capillary pressure, σ is the surface tension of the liquid, θ_c is the contact angle, $Z(\theta_c)$ is the Melrose function assumed to equal 1, and $J(s)$ is the Leverett function assumed to have a constant value of 0.53 [28].

Because capillary force becomes dominant in porous media, neglecting gravitational force produces the liquid velocity through the porous media:

$$\langle \widehat{u}_l \rangle = \frac{K^{1/2}}{2C_E\rho_l}\left[\left(\frac{\mu_l^2}{K^2} + \frac{2.12 C_E \rho_l \sigma}{K^{1/2}(K/\varepsilon)^{1/2} l_m}\right)^{1/2} - \frac{\mu_l}{K}\right] \tag{10}$$

Finally, the local rate of liquid supply from the porous layer to the heating surface is given as follows:

$$\dot{m} = \rho_l A_{po} \langle u_l \rangle \tag{11}$$

Based on the local energy balance between liquid entering the microporous layer and the sublayer, and the rate of the liquid depletion, the local CHF occurrence is defined as follows [29]:

$$\frac{q''_{CHF} A_w}{h_{fg}} = \rho_l \langle u_l \rangle \delta_m l + \rho_l \frac{K^{1/2}}{2C_E\rho_l}\left[\left(\frac{\mu_l^2}{K^2} + \frac{4 C_E \rho_l C_J \sigma}{K^{1/2}(K/\varepsilon)^{1/2} l_m}\right)^{1/2} - \frac{\mu_l}{K}\right]\varepsilon \delta_p l \tag{12}$$

Using the assumption of porosity and the diameter of porous particles as 0.6 nm and 250 nm, respectively, the

predicted CHF enhancement value by additional liquid supply of R-123 through the porous structure is 2.7 kW/m^2 from Eq. (12). The measured CHF enhancements are in the range of 17–44 kW/m^2 with increasing mass flow rate. The CHF value predicted by Yang's model shows a difference with the measured CHF value. Because the existing model was developed using the pool boiling concept, a modified model considering bulk liquid flow is needed to better predict CHF enhancement by porous structure. Because the bulk liquid velocity can determine the pressure difference through the porous media, it is suggested that the capillary pressure function may contain a bulk liquid velocity factor in itself like:

$$p_c = 0.53\frac{\sigma}{(K/\varepsilon)^{1/2}}f(u_l) \tag{13}$$

where $f(u_l)$ is a multiplier factor function of bulk liquid velocity.

Because of the insufficient experimental data and quantification of each parameter, a clearer explanation of the enhanced rewetting process by nanoparticles deposited on the surface could not be achieved exactly despite almost the same order of around 10^1 kW/m^2. With consideration of the bulk liquid velocity factor, further studies on CHF data for the various types of fluid and surface, and clear quantification of surface parameters such as porosity and the diameter of porous particles will be desirable.

The CHF enhancement phenomena in R-123 refrigerant on a bare and Al_2O_3 nanoparticle-coated heater were investigated according to mass flux. The nanoparticle-coated surface shows little difference in heat transfer coefficient, while CHF was enhanced up to 17% compared with the bare surface. Because of the high wettability of R-123 working fluid, the porosity and capillarity were assumed to be the key parameters for CHF enhancement. The porous structure of nanoparticles deposited on the surface provides the enhancement of the rewetting process induced by increased capillary action. The CHF value predicted by the existing theoretical model using capillary action through porous structure shows a difference with the measured CHF value. Because the existing model was developed using the pool boiling concept, a modified model considering bulk liquid flow is needed to better predict CHF enhancement by porous structures. Further studies on CHF data for the various types of fluid and surface and clear quantification of surface parameters such as porosity and the diameter of porous particles are needed.

Acknowledgments

This work was supported by the Nuclear Energy Research Program through the National Research Foundation of Korea (NRF) funded by the Ministry of Science, ICT, and Future Planning (2013M2A8A1041442, 2013M2B2B1075734, and 2013M2B2A4041473).

Nomenclature

The following symbols are used in this paper:

A_h	total heated surface area (m^2);
A_{po}	area of porous media (m^2);
C_E	Ergun coefficient;
$c_{p,f}$	heat capacity of liquid (kJ/kgK);
D_i	inner diameter of test section (m);
D_o	outer diameter of test section (m);
D	diameter of porous particle (m);
G	mass flux (kg/m^{2}s);
h_{fg}	latent heat of the liquid (kJ/kg);
I	current (A);
J	Leverett function;
K	absolute permeability tensor (m^2);
k_c	thermal conductivity (W/mK);
$L_{eff,h}$	effective heated length of the test section (m);
l_m	length of media (m);
m_f	mass flow rate (kg/s);
p_c	capillary pressure (Pa);
p_g	vapor pressure (Pa);
p_l	liquid pressure (Pa);
Q_{net}	net input power (W);
q''_{CHF}	critical heat flux (kW/m^2);
q''_{eff}	effective heat flux (kW/m^2);
T_{in}	liquid inlet temperature into the test section (°C);
T_L	local mean bulk temperature (°C);
T_{sat}	saturation temperature of liquid (°C);
T_{wall}	inner wall temperature (°C);
$T_{wall,out}$	outer wall temperature (°C);
$\langle u_l \rangle$	volume-averaged liquid velocity vector through the liquid-saturated region within the porous-layer coating (m/s);
V	voltage (V);
X_e	exit quality;
Z	Melrose function;
δ_p	porous coating layer thickness (m);
ε	porosity, or area fraction;
θ_c	static contact angle (°);
μ_l	dynamic viscosity of liquid (kg/ms);
ρ_l	liquid density (kg/m^3); and
σ	surface tension of the liquid (Ns/m^2).

Conflicts of interest

All contributing authors declare no conflicts of interest.

REFERENCES

[1] J. Buongiorno, L. Hu, S.J. Kim, R. Hannink, B. Truong, E. Forrest, Nanofluids for enhanced economics and safety of nuclear reactors: an evaluation of the potential features, issues, and research gaps, Nucl. Technol. 162 (2008) 80–91.
[2] J. Weisman, B.S. Pei, Prediction of critical heat flux inflow boiling at low quality, Int. J. Heat Mass Transf. 26 (1983) 1463–1477.
[3] C.H. Lee, I. Mudawwar, A mechanistic critical heat flux model for subcooled flow boiling based on local bulk flow conditions, Int. J. Multiphase Flow 14 (1988) 711–728.
[4] S.M. You, J.H. Kim, K.H. Kim, Effect of nanoparticles on critical heat flux of water in pool boiling heat transfer, Appl. Phys. Lett. 83 (2003) 3374–3376.

[5] P. Vassallo, R. Kumar, S. D'Amico, Pool boiling heat transfer experiments in silica-water nano-fluids, Int. J. Heat Mass Transf. 47 (2004) 407–411.
[6] I.C. Bang, S.H. Chang, Boiling heat transfer performance and phenomena of Al_2O_3-water nano-fluids from a plain surface in a pool, Int. J. Heat Mass Transf. 48 (2005) 2407–2419.
[7] D. Wen, Y. Ding, Experimental investigation into the pool boiling heat transfer of aqueous based γ-alumina nanofluids, J. Nanopart. Res. 7 (2005) 265–274.
[8] H. Kim, J. Kim, M. Kim, Experimental study on CHF characteristics of water-TiO_2 nanofluids, Nucl. Eng. Technol. 38 (2006) 61–68.
[9] S.J. Kim, I.C. Bang, J. Buongiorno, L.W. Hu, Surface wettability change during pool boiling of nanofluids and its effect on critical heat flux, Int. J. Heat Mass Transf. 50 (2007) 4105–4116.
[10] S.J. Kim, T. McKrell, J. Buongiorno, L.W. Hu, Alumina nanoparticles enhance the flow boiling critical heat flux of water at low pressure, J. Heat Transf. 130 (2008), 044501-1–;044501–3.
[11] S.J. Kim, T. McKrell, J. Buongiorno, L.W. Hu, Experimental study of flow critical heat flux in alumina-water, zinc-oxide-water, and diamond-water nanofluids, J. Heat Transf. 131 (2009), 043204-1–;043204–7.
[12] T.I. Kim, Y.H. Jeong, S.H. Chang, An experimental study on CHF enhancement in flow boiling using Al_2O_3 nano-fluid, Int. J. Heat Mass Transf. 53 (2010) 1015–1022.
[13] S.W. Lee, S.D. Park, S. Kang, S.M. Kim, H. Seo, D.W. Lee, I.C. Bang, Critical heat flux enhancement in flow boiling of Al_2O_3 and SiC nanofluids under low pressure and low flow conditions, Nucl. Eng. Technol. 44 (2012) 429–436.
[14] J. Chen, On the Interaction between Fuel CRUD and Water Chemistry in Nuclear Plants, SKI Report 00:5, Studsvik, Nyköping, Sweden, 2000.
[15] I.C. Bang, J.H. Kim, Thermal-fluid characterizations of ZnO and SiC nanofluids for advanced nuclear power plants, Nucl. Technol. 170 (2010) 16–27.
[16] J. Buongiorno, Can corrosion and CRUD actually improve safety margins in nuclear plants?, in: 8th International Conference on Multiphase Flow, May 26–31, Korea, Jeju, 2013, pp. 9–21.
[17] M.S. Sarwar, Y.H. Jeong, S.H. Chang, Subcooled flow boiling CHF enhancement with porous surface coatings, Int. J. Heat Mass Transf. 50 (2007) 3649–3657.
[18] B. Truong, L.W. Hu, J. Buongiorno, T. McKrell, Alumina nanoparticle pre-coated tubing enhancing subcooled flow boiling critical heat flux, in: Proceedings of the ASME 2009 2nd Micro/Nanoscale Heat & Mass Transfer International Conference, Dec 18–21, Shanghai, China, 2009, pp. 533–539.
[19] T.I. Kim, W.J. Chang, S.H. Chang, Flow boiling CHF enhancement using Al_2O_3 nanofluid and an Al_2O_3 nanoparticle deposited tube, Int. J. Heat Mass Transf. 54 (2011) 2021–2025.
[20] A. Kosar, Y. Peles, Critical heat flux of R-123 in silicon-based microchannels, J. Heat Transf. 129 (2007) 844–851.
[21] A.P. Roday, M.K. Jensen, Study of the critical heat flux condition with water and R-123 during flow boiling in microtubes. Part I: experimental results and discussion of parametric effects, Int. J. Heat Mass Transf. 52 (2009) 3235–3249.
[22] A.P. Roday, M.K. Jensen, Study of the critical heat flux condition with water and R-123 during flow boiling in microtubes. Part II: Comparison of data with correlations and establishment of a new subcooled CHF correlation, Int. J. Heat Mass Transf. 52 (2009) 3250–3256.
[23] H. Seo, J.H. Chu, S.Y. Kwon, I.C. Bang, Pool boiling CHF of reduced graphene oxide, graphene, and SiC-coated surfaces under highly wettable FC-72, Int. J. Heat Mass Transf. 82 (2015) 490–502.
[24] M.T. Al-Garni, B.D. Al-Anazi, Investigation of wettability effects on capillary pressure, and irreducible saturation for Saudi crude oils, using rock centrifuge, Oil Gas Bus. J. (2008) 1–17.
[25] K.M. Kim, S.W. Lee, I.C. Bang, Effects of SiC and Graphene-oxide Nanoparticles-coated Surfaces on Quenching Performance, ATH2014, Jun 15–19, Reno, NV, 2014, pp. 484–495.
[26] S. Fischer, E.M. Slomski, P. Stephan, M. Oechsner, Enhancement of nucleate boiling heat transfer by micro-structured chromium nitride surfaces, J. Phys. Conf. Ser. 395 (2012) 012128.
[27] M. Kaviany, Principles of Heat Transfer in Porous Media, Springer, New York, 1999.
[28] S.G. Liter, M. Kaviany, Pool-boiling CHF enhancement by modulated porous-layer coating: theory and experiment, Int. J. Heat Mass Transf. 44 (2001) 4287–4311.
[29] J. Yang, F.B. Cheung, A hydrodynamic CHF model for downward facing boiling on a coated vessel, Int. J. Heat Fluid Flow 26 (2005) 474–4841.